

# Unlocking the Potential of Magnetotactic Bacteria as Magnetic Hyperthermia Agents

David Gandia, Lucía Gandarias, Irati Rodrigo, Joshua Robles-García, Raja Das, Eneko Garaio, José Ángel García, Manh-Huong Phan, Hariharan Srikanth, Iñaki Orue, Javier Alonso,\* Alicia Muela,\* and M<sup>a</sup> Luisa Fdez-Gubieda\*

Magnetotactic bacteria are aquatic microorganisms that internally biomineralize chains of magnetic nanoparticles (called magnetosomes) and use them as a compass. Here it is shown that magnetotactic bacteria of the strain *Magnetospirillum gryphiswaldense* present high potential as magnetic hyperthermia agents for cancer treatment. Their heating efficiency or specific absorption rate is determined using both calorimetric and AC magnetometry methods at different magnetic field amplitudes and frequencies. In addition, the effect of the alignment of the bacteria in the direction of the field during the hyperthermia experiments is also investigated. The experimental results demonstrate that the biological structure of the magnetosome chain of magnetotactic bacteria is perfect to enhance the hyperthermia efficiency. Furthermore, fluorescence and electron microscopy images show that these bacteria can be internalized by human lung carcinoma cells A549, and cytotoxicity studies reveal that they do not affect the viability or growth of the cancer cells. A preliminary in vitro hyperthermia study, working on clinical conditions, reveals that cancer cell proliferation is strongly affected by the hyperthermia treatment, making these bacteria promising candidates for biomedical applications.


## 1. Introduction

More than 100 years ago, Paul Ehrlich, the founder of chemotherapy, already postulated the creation of “magic bullets” in order to use them in the fight against human diseases.<sup>[1]</sup> Later, in the late 1950s, this idea was recovered by Richard Feynman, whom proposed the possibility of using nanorobots as tiny “surgeons” capable of navigating inside the human body, locating damaged cells or tissues, and “fixing” them as needed.<sup>[2]</sup> This originally considered “wild idea” has quickly evolved from the speculative realm of science fiction stories to become the main research area in many laboratories across the world. Different kinds of “nanosurgeons” or “nanorobots” are being investigated nowadays such as those based on inorganic nanoparticles, bacteria and virus, DNA structures, etc.<sup>[3–6]</sup> In particular, in the last decades, much of the

D. Gandia, I. Rodrigo, Prof. J. Á. García, Prof. A. Muela, Prof. M. L. Fdez-Gubieda  
Basque Center for Materials  
Applications and Nanostructures (BCMaterials)  
UPV/EHU Science Park  
Leioa 48940, Spain  
E-mail: alicia.muela@ehu.eus; malu.gubieda@ehu.eus

L. Gandarias, Prof. A. Muela  
Departamento de Inmunología  
Microbiología y Parasitología  
Universidad del País Vasco (UPV/EHU)  
Leioa 48940, Spain

J. Robles-García, Prof. R. Das, Prof. M.-H. Phan, Prof. H. Srikanth  
Materials Institute  
Department of Physics  
University of South Florida (USF)  
Tampa, FL 33620, USA

 The ORCID identification number(s) for the author(s) of this article can be found under <https://doi.org/10.1002/sml.201902626>.

© 2019 The Authors. Published by WILEY-VCH Verlag GmbH & Co. KGaA, Weinheim. This is an open access article under the terms of the Creative Commons Attribution License, which permits use, distribution and reproduction in any medium, provided the original work is properly cited. The copyright line for this article was changed on 19 October 2019 after original online publication.

DOI: 10.1002/sml.201902626

Prof. E. Garaio, Prof. J. Á. García  
Departamento de Física Aplicada II  
Universidad del País Vasco (UPV/EHU)  
Leioa 48940, Spain

Prof. E. Garaio  
Departamento de Ciencias  
Universidad Pública de Navarra (UPN)  
Pamplona 31006, Spain

Dr. I. Orue  
SGIker Medidas Magnéticas  
Universidad del País Vasco (UPV/EHU)  
Leioa 48940, Spain

Prof. J. Alonso  
Departamento CITIMAC  
Universidad de Cantabria (UC)  
Santander 39005, Spain  
E-mail: alonsomasaj@unican.es

Prof. M. L. Fdez-Gubieda  
Departamento de Electricidad y Electrónica  
Universidad del País Vasco (UPV/EHU)  
Leioa 48940, Spain

work has been focused on the use of magnetic nanoparticles as theranostic nanorobots, especially in the field of cancer detection and treatment.<sup>[7–10]</sup> These nanoparticles can be easily synthesized in the laboratory and they present a series of promising characteristics for their use as nanorobots. Their small size (5–100 nm) allows them to interact with cancer cells, their biocompatibility (e.g., iron oxide nanoparticles) minimizes adverse reactions when introduced inside the human body, and most important, their magnetic properties can be employed to manipulate them remotely and make them actuate when in the tumor area.<sup>[11,12]</sup> In this way, novel strategies based on the use of magnetic nanoparticles have emerged for improving the detection of tumors (magnetic resonance imaging contrast agents, magnetic particle imaging, etc.) and their elimination (drug delivery, mechanical nanoactuation, magnetic hyperthermia, photothermia, etc.)<sup>[9,13–16]</sup>

Despite all this research, we are still, unfortunately, far from a standardized clinical implementation of magnetic nanoparticles. There are several issues and limitations that are intrinsic to the nature of these nanoparticles, such as their lack of self-propelled mobility and environment sensing mechanisms, their tendency to become agglomerated inside the tumors, their low targeting efficiency when injected intravenously, the difficulties for removing them from the body after the treatment is finished, etc. In order to overcome these and other difficulties, different alternative nanorobots have been proposed in the last few years. Among them, the idea of using biological entities such as virus or bacteria to interact with tumors has been gaining momentum.<sup>[17,18]</sup>

In a recent article by Forbes,<sup>[19]</sup> it was stated that the perfect cancer therapy nanorobots should be able to perform several important functions: target tumors, produce and/or transport cytotoxic molecules, self-propel, sense the local environment and be detectable, etc. Bacteria in general have biological mechanisms to perform these functions: flagella to self-propel, specific regions to respond to external signals, chemotaxis receptors, machinery to produce detectable molecules, etc. but they lack the magnetic response and actuation properties that have made magnetic nanoparticles so attractive for biomedical applications in general and cancer treatment in particular.

Fortunately, there is a particular group of bacteria that combine the best of both worlds: the so-called “Magnetotactic bacteria” (see **Figure 1**).<sup>[20,21]</sup> Magnetotactic bacteria are aquatic microorganisms that swim along the Earth’s magnetic field lines using chains of nanoparticles biomineralized internally (called magnetosomes) as compass. The different species of magnetotactic bacteria synthesize chains of perfectly stoichiometric magnetite nanocrystals, with genetically controlled sizes and shapes, surrounded by a biocompatible membrane.

Since the magnetotactic bacteria can sense magnetic fields, they can be externally detected, manipulated and guided, and they can also be potentially used for both detection and treatment of cancer through MRI, magnetic hyperthermia, or drug delivery.<sup>[22–26]</sup> Moreover, magnetotactic bacteria prefer to live in low oxygen concentration regions in water. Since the tumor area is low in oxygen, targeting tumors with these bacteria becomes easier and more efficient than with nanoparticles or with other bacteria. Therefore, magnetotactic bacteria present themselves as the paradigm of efficient nanorobots for cancer treatment. We will refer to them as “nanobiots.”

In the last years, a few groups have started to investigate the possibility of using magnetotactic bacteria as nanobiots for cancer treatment.<sup>[23,24,27,28]</sup> These groups have focused mainly on tracking and analyzing the movement of bacteria in different environments,<sup>[29]</sup> studying the potential penetration of bacteria into tumors,<sup>[30]</sup> developing novel magnetic systems to remotely control and guide these bacteria,<sup>[31]</sup> analyzing their biocompatibility and navigation in blood stream,<sup>[32]</sup> etc. The initial results have been very positive and there have already been in vivo tests demonstrating the efficiency of these bacteria in tumors targeting.<sup>[22]</sup>

In the present work, we want to test magnetotactic bacteria as nanobiots for cancer treatment by analyzing their performance as magnetic hyperthermia agents. Magnetic hyperthermia is a process in which controlled heating of magnetic nanoparticles located in the tumor can kill or deactivate cancer cells.<sup>[13,33,34]</sup> The superior magnetic properties of magnetosomes in magnetic hyperthermia have already been reported.<sup>[35,36]</sup> However, the number of works on magnetic hyperthermia performance of the “whole” magnetotactic bacteria is very limited. Song et al.<sup>[37]</sup> found that magnetotactic bacteria under an external alternating magnetic field (AMF) can be used to kill *Staphylococcus aureus*, a common hospital and household pathogen. And Alphandéry et al.<sup>[26]</sup> showed that intact bacterial cells containing chains of magnetosomes exhibit high specific absorption rates (SARs) of 625 W g<sup>−1</sup> at 880 Oe and 108 kHz.

Although the initial results seem promising, a more thorough analysis is necessary in order to fully harness the power of magnetotactic bacteria in the fight against cancer. Therefore, we have carried out a comprehensive study of the hyperthermic response of *Magnetospirillum gryphiswaldense* MSR-1 strain under different conditions: AC field and frequency, alignment of the bacteria, medium viscosity, etc. Their heating efficiency has been measured using both calorimetric and AC magnetometry methods.<sup>[33,38]</sup> The combination of both techniques is quite unusual, due to the lack of commercial systems that can carry out AC magnetometry hyperthermia, and has allowed us not only to check the performance of magnetotactic bacteria as heating agents (calorimetric method) but also to better

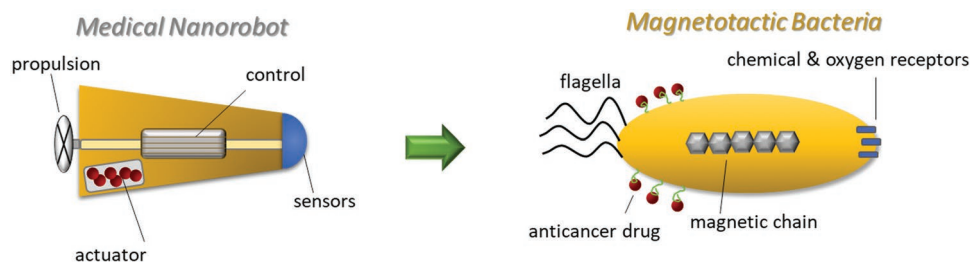


**Figure 1.** Description of the features that a medical nanorobot must exhibit for cancer treatment and the characteristics of a magnetotactic bacterium functionalized with anticancer drugs.

understand the mechanisms behind their heating efficiency and how to optimize it (AC magnetometry). Our experimental results reveal that these bacteria exhibit superb heating efficiency, close to that expected for an “ideal” heating mediator, provided their alignment with the magnetic field is efficiently controlled. In addition, we have also studied the internalization, the cytotoxicity, and the effect of the hyperthermia treatment of these bacteria in the presence of A549 human lung carcinoma cells, finding that magnetotactic bacteria can be efficiently internalized by cancer cells, exhibiting very low cytotoxicity and affecting the cell proliferation after magnetic hyperthermia treatment. To the best of our knowledge, this is the first time that such a thorough experimental study has been carried out.

## 2. Results and Discussion

As depicted in **Figure 2**, *M. gryphiswaldense* MSR-1 bacteria present spirillum shape (2–5  $\mu\text{m}$  length and 0.5  $\mu\text{m}$  width), with a long chain of magnetosomes inside. It has been reported that their small size allow these bacteria to navigate through blood vessels, penetrate in tumors, and interact with them.<sup>[30,39]</sup> In addition, the inset shows that these bacteria have a flagellum at each end of their body, which allows them to propel in liquid media at speeds often exceeding 25  $\mu\text{m s}^{-1}$ .<sup>[40]</sup> These characteristics are ideal for their use as nanobiots for cancer treatment. The magnetic response of magnetotactic bacteria has also been characterized in our previous works.<sup>[41]</sup> The magnetization versus temperature curves present a well-defined Verwey transition around 110 K, which is a clear cut indicator of the stoichiometric magnetite structure of magnetosomes, the low dispersion on their size, and thereby, of their enhanced magnetic response.

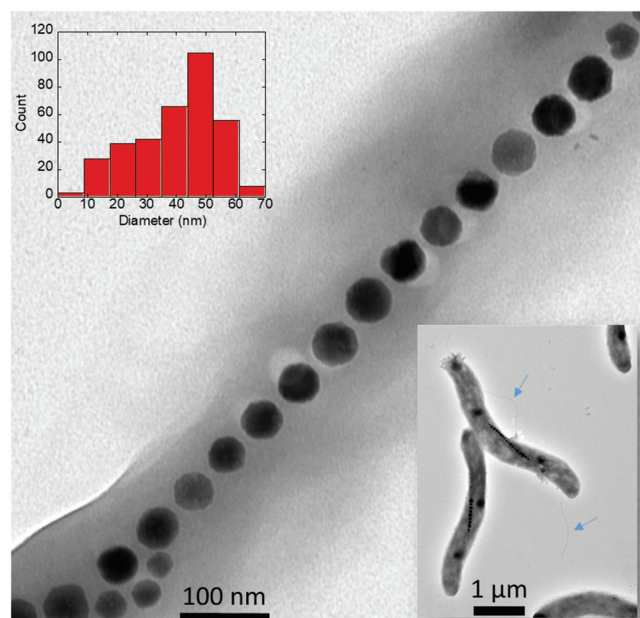


**Figure 2.** TEM image of the chain of magnetosomes inside *M. gryphiswaldense* MSR-1 bacteria. A histogram with the size distribution of magnetosomes has been included. In the inset, the whole bacteria are shown, and their flagella are indicated with blue arrows.

### 2.1. Magnetic Hyperthermia

The main idea in hyperthermia mediated treatment of cancer is that, by raising the temperature of cancer cells up to a “therapeutic window” typically between 40 and 44  $^{\circ}\text{C}$ , they can be deactivated (dead or driven to apoptosis) without affecting the healthy tissue. This is possible because in this range of temperatures, cancer cells have been shown to be more susceptible to heat than healthy ones.<sup>[13]</sup> In addition, it has also been shown that by rising the temperature cancer cells become more susceptible to radio or chemotherapy<sup>[42,43]</sup> thus improving the efficiency of these therapies. If we raise the temperature up to values higher than 50  $^{\circ}\text{C}$ , a more violent (and less safe) cancer cell death is induced through thermal ablation.<sup>[44]</sup>

In Magnetic Hyperthermia, the heating of the nanoparticles is produced by applying an alternating magnetic field with a define amplitude,  $H$ , and frequency,  $f$ . As reported before, the heating efficiency of our bacteria has been measured by calorimetric and AC magnetometry methods.

Calorimetric measurements (**Figure 3**) carried out at 300 kHz in water clearly indicate that magnetotactic bacteria can raise the temperature of the medium easily reaching the therapeutic window in just 3 min, by applying AC fields  $\geq 300$  Oe (initial body temperature, 37  $^{\circ}\text{C}$ ). Below 200 Oe, the heating is practically negligible for the bacteria concentration used ( $\approx 9 \times 10^9$  bacteria  $\text{mL}^{-1} \approx 0.15$   $\text{mg}_{\text{Fe}_3\text{O}_4} \text{mL}^{-1}$ ). This suggests that magnetotactic bacteria can be used as efficient heating agents by applying high enough AC fields. If a more drastic destruction of the cancer cells through thermal ablation was desired, higher fields and longer exposure times would let us increase the temperature above 50  $^{\circ}\text{C}$  (thermal ablation), as shown in Figure 3 (although safety limits for maximum field applicable should be taken into consideration<sup>[45]</sup>).

Once the magnetotactic bacteria are inside the tumor area, their movement would be more restricted than in the blood vessels or in water, as in the previous results. In order to investigate how this would affect their heating properties, we have repeated the magnetic hyperthermia measurements this time in a more viscous medium, made of water with 2% agar. Moreover, we have also compared how the heating in this viscous medium varies if the bacteria are randomly dispersed or aligned parallel to the applied magnetic field. The corresponding heating curves are also presented in Figure 3.

We can see that, when the bacteria are in the 2% agar medium and aligned parallel to the AC field, the obtained heating curves are very similar to those previously measured in water. This suggests that the bacteria in water align in the direction of the applied field, as expected due to magnetotaxis effect. However, heating rates decrease when the bacteria are randomly oriented and cannot align with the field. This indicates that in order to optimize the heating of magnetotactic bacteria for their use as hyperthermic nanobiots, they need to be as aligned as possible in the direction of the AC field during the hyperthermia treatment. Despite this, it must be remarked that even when the bacteria are randomly oriented, we can also reach temperatures inside the tumor within the therapeutic window for AC fields  $\geq 300$  Oe at 300 kHz.

In order to compare the heating efficiency of magnetotactic bacteria with those reported in the literature for other similar

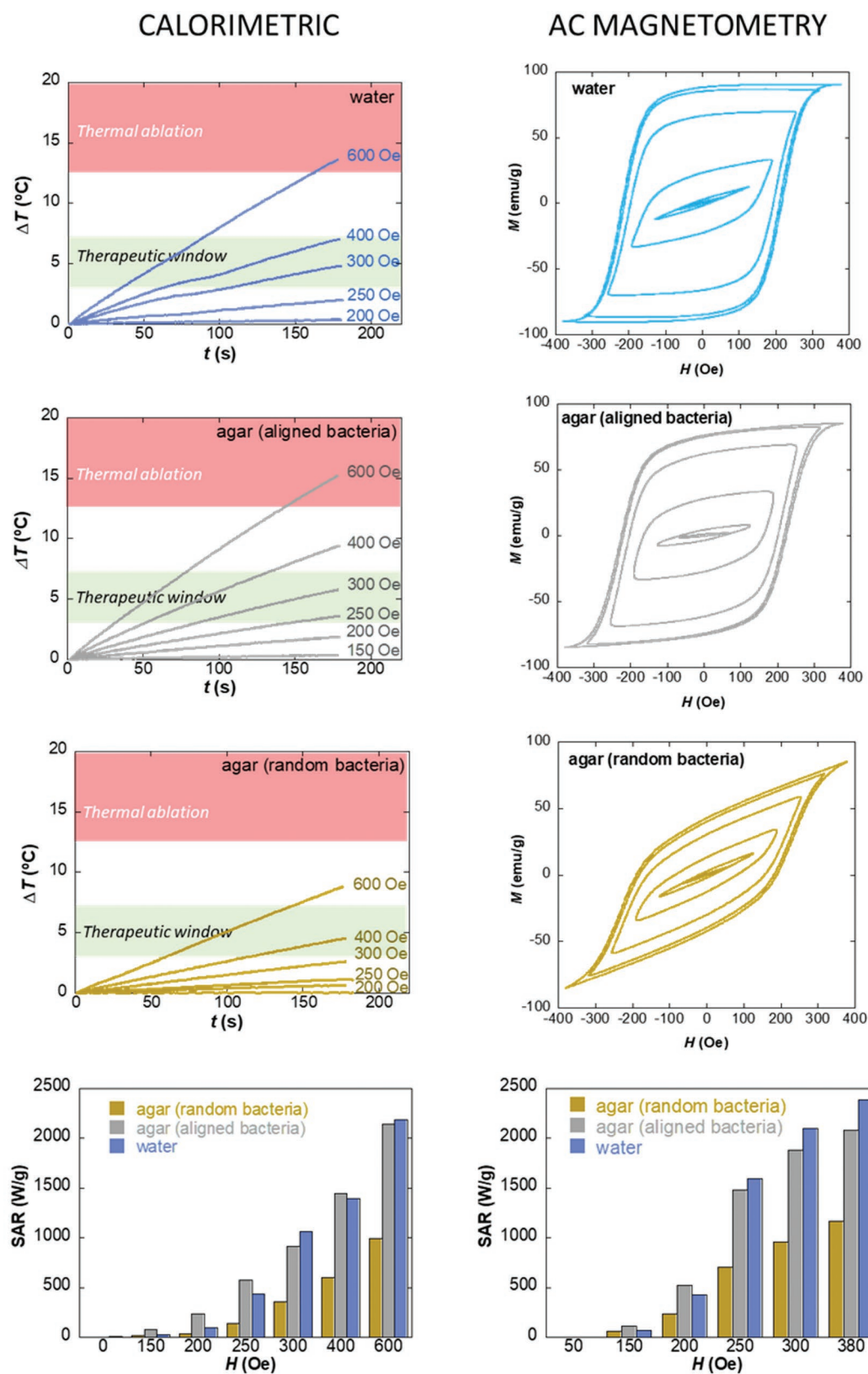


**Figure 3.** Left column: Heating curves, Temp versus time; right column: AC hysteresis loops,  $M$  versus  $H$ , of magnetotactic bacteria in water, 2% agar aligned, and 2% agar random, measured at AC fields 0–600 Oe and 300 kHz. In addition, the SAR values obtained from the heating curves and hysteresis loops are also represented.



magnetic nanosystems, we can calculate the so-called “specific absorption rate (SAR)” or “specific loss power (SLP).” The heating efficiency or SAR is directly related to the initial slope of the heating curves<sup>[46]</sup>

$$\text{SAR} = \frac{m_s}{m_n} C_p \frac{\Delta T}{\Delta t} \quad (1)$$

where  $C_p$  is the specific heat of the solvent,  $m_s$  is the mass of the solvent,  $m_n$  is the mass of the nanoparticles, and  $\Delta T/\Delta t$  is the initial slope of the heating curves (as obtained from the linear fitting of the heating curves during the first few seconds). As can be seen in Figure 3, the obtained SAR values reach over  $2000 \text{ W g}^{-1}$  for the highest AC field amplitude applied (600 Oe) and a frequency of 300 kHz.

It is clear from these hyperthermia measurements that the alignment plays an important role in the heating efficiency of our magnetotactic bacteria. In order to better understand the role of the alignment and the mechanisms behind the high heating efficiency of our bacteria, we have also carried out AC magnetometry measurements. In AC magnetometry, the AC hysteresis loops are measured, and the heating efficiency is directly obtained from the area of the loops (hysteresis losses). This means that, essentially, the bigger the area of the AC loops, the better the heating efficiency. Therefore, it is easy to realize that the optimum shape of the AC loops in order to maximize the hysteresis losses would be a rectangular shape with high squareness, i.e., high coercivity and remanence. Computer simulations carried out by different groups<sup>[47–49]</sup> suggest that aligned chain-like structures of magnetic nanoparticles, exhibiting a well-defined anisotropy axis, could give rise to AC loops that resemble this optimum shape. This has also been supported by the experimental results obtained in highly anisotropic nanostructures, such as magnetite nanorods.<sup>[50]</sup> Unfortunately, assembling this kind of chains and preventing them from collapsing is not an easy task, due to, among other factors, the presence of attractive magnetic interactions between chains. To this respect, magnetotactic bacteria present a clear advantage: they already present a stable chain of magnetosomes, and since these magnetic chains are “embedded” inside the bacteria (see Figure 2), they are efficiently separated by the bacterial mass, thereby avoiding the effect of magnetic interactions.

The AC hysteresis loops measured for MSR-1 bacteria have been represented in Figure 3. There are several interesting things to point out concerning the evolution of the AC loops. With increasing field, the AC loops evolve from the typical lancet shape of a minor loop at  $H \leq 100 \text{ Oe}$  (extremely narrow, with low squareness and low maximum magnetization), to a rectangular loop, for  $H \geq 250 \text{ Oe}$ , close to the optimum shape described before when the bacteria area parallel to the field. This confirms that bacteria, when aligned in the direction of the AC field, behave as an ideal magnetic hyperthermia mediators, supporting previous simulations. When the bacteria are randomly oriented the AC loops are tilted and do not saturate, giving rise to lower hysteresis losses. This can be related to the increase of the effective anisotropy field as the bacteria deviate from the parallel orientation.<sup>[38,50,51]</sup>

In addition, AC loops of magnetotactic bacteria dispersed in water greatly resemble those of oriented magnetotactic bacteria

in agar: coercive field is virtually the same and magnetization remanence is only a little bit smaller in agar. This suggests that an AC field of hundreds of kHz acts as a very efficient mechanical anchor for magnetotactic bacteria: magnetization reversal in water is driven by intrinsic dynamical processes, just like in fixed (or nearly immobilized) bacteria. Small differences between water and agar (with oriented samples) would reflect basically different orientation degree. As a consequence, physical rotation (Brownian relaxation) of the chain of magnetosomes seems to play a very minor role in the heating efficiency of magnetotactic bacteria. This is not surprising, noting that magnetosome chains are embedded inside bacteria whose response velocity to external fields is much lower than that required to follow kilohertz excitations. This feature indicates that, contrary to what frequently happens with inorganic magnetic nanoparticles,<sup>[34]</sup> magnetotactic bacteria will still be able to provide high heating efficiency after penetrating and getting immobilized inside the tumor.

The SAR values (in  $\text{W g}^{-1}$ ), as commented before, were directly obtained from the area ( $A$ ) of the AC hysteresis loops, according to Equation (2)<sup>[46]</sup>

$$\text{SAR} \left( \frac{\text{W}}{\text{g}} \right) = \frac{f}{c} \cdot A = \frac{f}{c} \cdot \oint \mu_0 M_t dH_t \quad (2)$$

with  $M_t$  being the instantaneous magnetization at time  $t$ ,  $H_t$  the sinusoidal magnetic field of frequency  $f$  at time  $t$ , and  $c$  the magnetite weight concentration in the dispersing medium. The integration is done over a period of the oscillating magnetic field,  $T = 2\pi/f$ .

It must be noted that the SAR value obtained from AC magnetometry,  $\approx 2400 \text{ W g}^{-1}$  at 380 Oe, is appreciably higher than the one estimated before from the calorimetric measurements,  $\approx 1400 \text{ W g}^{-1}$  at 400 Oe, both measured at a frequency of 300 kHz. This divergence can be easily understood considering that in the case of calorimetric measurements, we are deriving the heating efficiency of the nanoparticles from the average temperature measured in the medium. If there is enough concentration of magnetic material in the medium, the temperatures reached in the medium and on the surface of the nanoparticles are going to be similar. However, at low concentrations of magnetic material, the temperature in the medium is going to be lower than the one reached on the surface of the nanoparticles, and thereby, the SAR values obtained from measuring the temperature of the medium are going to be smaller than those indicated by AC magnetometry measurements. In our case, even if the concentration of bacteria employed is relatively high ( $9 \times 10^9 \text{ cells mL}^{-1}$ ), the concentration of magnetic material is quite small, only  $0.15 \text{ mg-Fe}_3\text{O}_4 \text{ mL}^{-1}$  since these bacteria occupy a much larger volume than the one occupied by the nanoparticles. Increasing the applied field or the concentration of bacteria would diminish this problem. Another possibility would be to increase the number of chains and/or magnetosomes per cell, something that in fact, has already been proved to be feasible.<sup>[52,53]</sup>

We commented before that using magnetotactic bacteria instead of inorganic nanoparticles for magnetic hyperthermia treatment had a series of advantages, mainly related to their capacity to self-propel, sense the local environment, be remotely

guided, etc. It is important to remark that on top of that, the heating efficiency we obtain from magnetotactic bacteria is appreciably higher than the one we would obtain from the isolated magnetosomes. This can be clearly seen if we compare the SAR results obtained from AC magnetometry measurements for both magnetotactic bacteria and isolated magnetosomes dispersed in water, in the same conditions of magnetic material concentration,  $0.15 \text{ mg-Fe}_{304} \text{ mL}^{-1}$  (see Figure 4).

Figure 4 displays the evolution of the SAR values normalized by the frequency,  $f$ , for different magnetic field frequencies, as a function of the applied magnetic field amplitude,  $H$ , for magnetotactic bacteria and magnetosomes dispersed in water. We can obtain relevant information based on the experimental data. First of all, we see how the SAR values for both magnetotactic bacteria and magnetosomes increase linearly with the magnetic field frequency, since the normalized magnetic losses,  $\text{SAR}/f$ , are almost independent of the applied frequency, as we had already observed in our previous work on isolated magnetosomes.<sup>[35]</sup> Second, the SAR values for the magnetosomes dispersed in water are clearly lower than those obtained for magnetotactic bacteria. While with magnetosomes we reach values of  $\text{SAR}/f$  close to  $5 \text{ W g}^{-1} \text{ kHz}^{-1}$ , with magnetotactic bacteria we can reach values around  $8 \text{ W g}^{-1} \text{ kHz}^{-1}$ . As we have explained, this is originated by the easy alignment of the bacteria with the applied AC magnetic field, giving rise to a higher squareness of the hysteresis loops, as clearly depicted in the inset to Figure 4. And third, the evolution of the SAR curves as a function of the applied field for both magnetosomes and magnetotactic bacteria follows a similar trend, being negligible below a certain threshold field (which lies around 200 Oe in this case). As we pointed out in our previous works,<sup>[35,54]</sup> this is a clear hallmark of intrinsic hysteresis losses (which can be modeled by a Stoner–Wohlfarth approach) being the main mechanism of the heat production.

It must be remarked that the SAR values we are obtaining for these bacteria compare very well with some of the highest SAR values reported in the literature for iron oxide based nanoparticles.<sup>[34]</sup> For example, Guardia et al. reported SAR values of  $1000 \text{ W g}^{-1}$  for magnetite nanocubes measured at 275 Oe and 325 kHz, and we are also obtaining similar SAR values (from calorimetric measurements) at 300 Oe and

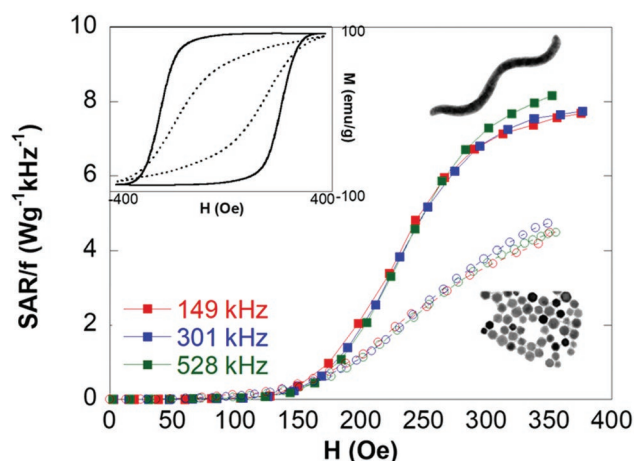


**Figure 4.** SAR normalized by the frequency,  $\text{SAR}/f$ , measurements at different frequencies, 149, 301, and 528 kHz, for bacteria and magnetosomes dispersed in water. Magnetosomes curve data has been taken from our previous work.<sup>[35]</sup> In the inset, AC hysteresis loops are presented corresponding to the bacteria (continuous line) and magnetosomes (dashed line) as obtained from AC magnetometry measurements (300 kHz).

300 kHz.<sup>[55]</sup> This indicates that magnetotactic bacteria can heat as well as some of the best iron oxide based nanoparticles reported in the literature for magnetic hyperthermia applications. As expected, the SAR values obtained for the randomly oriented bacteria diminish, although they still compare well with most of the SAR values reported in the literature for iron oxide nanoparticles.<sup>[38]</sup> We also have to take into account the possibility that SAR values of bacteria could diminish after internalization in cancer cells, as has been frequently reported for magnetic nanoparticles.<sup>[16,33]</sup> Therefore, it is important to test the capability of the bacteria as hyperthermia agents in *in vitro* experiments.

Concerning the field amplitudes and frequencies we are applying in this study, we must clarify that in the literature it is usually considered that the product of the amplitude  $\times$  frequency should be below a certain safety limit,  $H \cdot f \leq 5 \times 10^9 \text{ A m}^{-1} \text{ s}$ ,<sup>[45]</sup> for medical applications. This would imply that, for example, at 150 kHz, we should not apply more

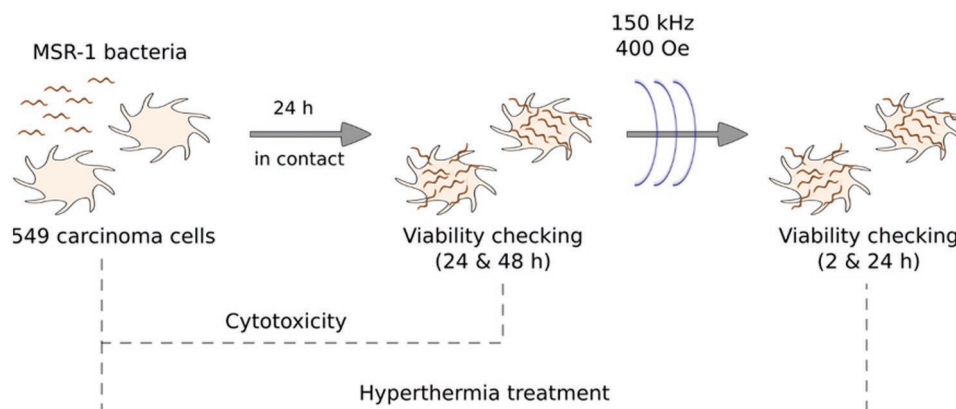


**Figure 5.** Scheme of *in vitro* assay carried out to determine the potential cytotoxic effect of *M. gryphiswaldense* MSR-1 and the effect of hyperthermia treatment in human lung carcinoma cells.

than  $\approx 400$  Oe for clinical hyperthermia, these are the conditions that we have used in the present work for studying the effect of hyperthermia treatment on lung cancer cells. This could restrict the heating capacity of our nanobiots, but it must be noted that there is still an ongoing discussion about the validity of this limit, and some works have suggested that, depending on the area of the tissue treated, the safety limit can reach values up to  $\approx 10^{10}$  A m $^{-1}$  s $^{-1}$ , the same order of magnitude than most of our measurements.<sup>[13]</sup>

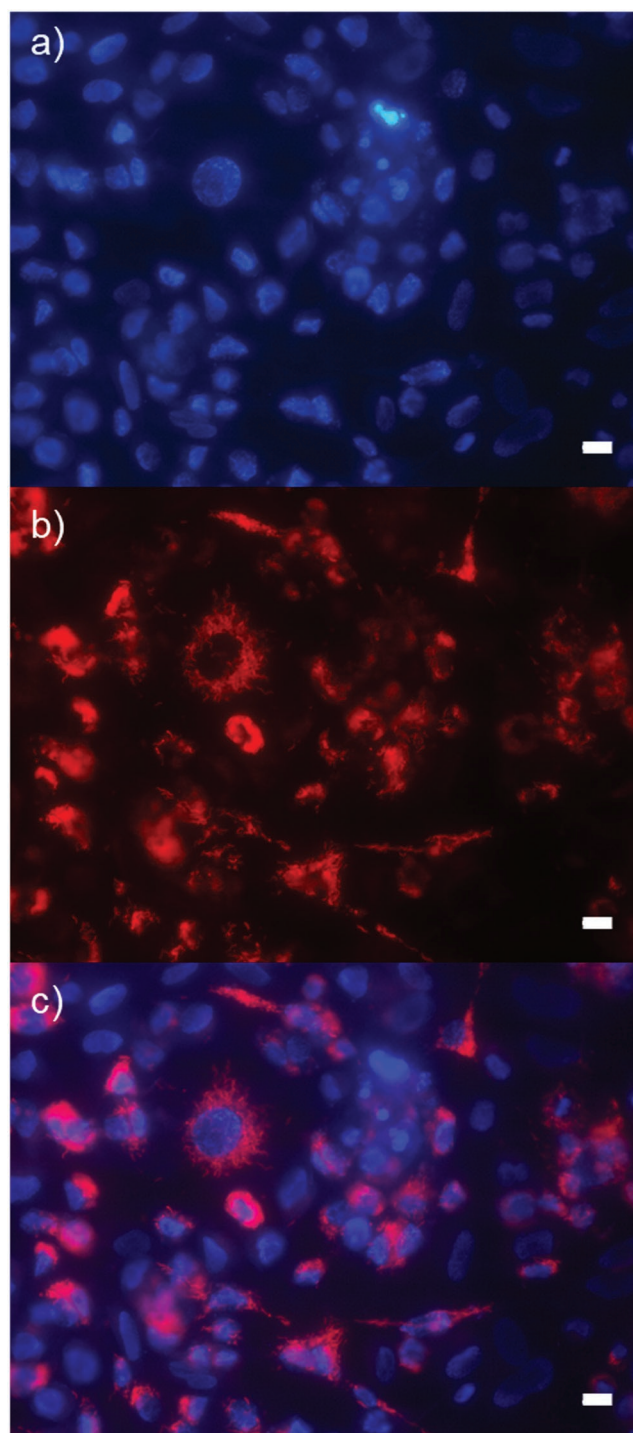
One of the most interesting advantages offered by the possibility of using AC magnetometry to measure SAR is that, as we have seen, it provides us with much more information in order to explain the experimental results. In fact, in our case, the measurement of the AC loops has allowed us to understand why the magnetic behavior of magnetotactic bacteria is ideal for increasing the heating efficiency during magnetic hyperthermia. To this day, very large efforts are being made to try to improve heating efficiency by controlling the synthesis techniques, such as modifying the size of the particles, their shape, trying to improve the saturation magnetization of the particle, etc. In our opinion, our results clearly demonstrate that the biological structure of the magnetosome chain of magnetotactic bacteria is perfect to enhance the hyperthermia efficiency. This not only supports the use of these bacteria as biological nanobiots with high efficiency for magnetic hyperthermia but also allows the study of the adequate parameters to increase the SAR values in other types of nanostructures with controlled arrangement.<sup>[56,57]</sup>

In addition, we would like to remark that the magnetotactic bacteria presented in this work have also high potential in other biomedical applications, such as magnetic particle imaging (MPI) agents. MPI is a novel medical imaging technique that relies on the nonlinearities of the time varying magnetization, and high order harmonics are used to map the position of the magnetic nanoparticles.<sup>[58]</sup> The highly squared AC hysteresis loops measured for the aligned bacteria (see Figure 3) present a high harmonic distortion on odd harmonics (3rd, 5th, 7th, ...), thus making these magnetotactic bacteria very promising candidates for MPI. The suitability of isolated bacterial magnetosomes as MPI tracer has already been reported in the literature.<sup>[59]</sup>

## 2.2. Bacterial Interaction with Cancer Cells and In Vitro Hyperthermia Treatment

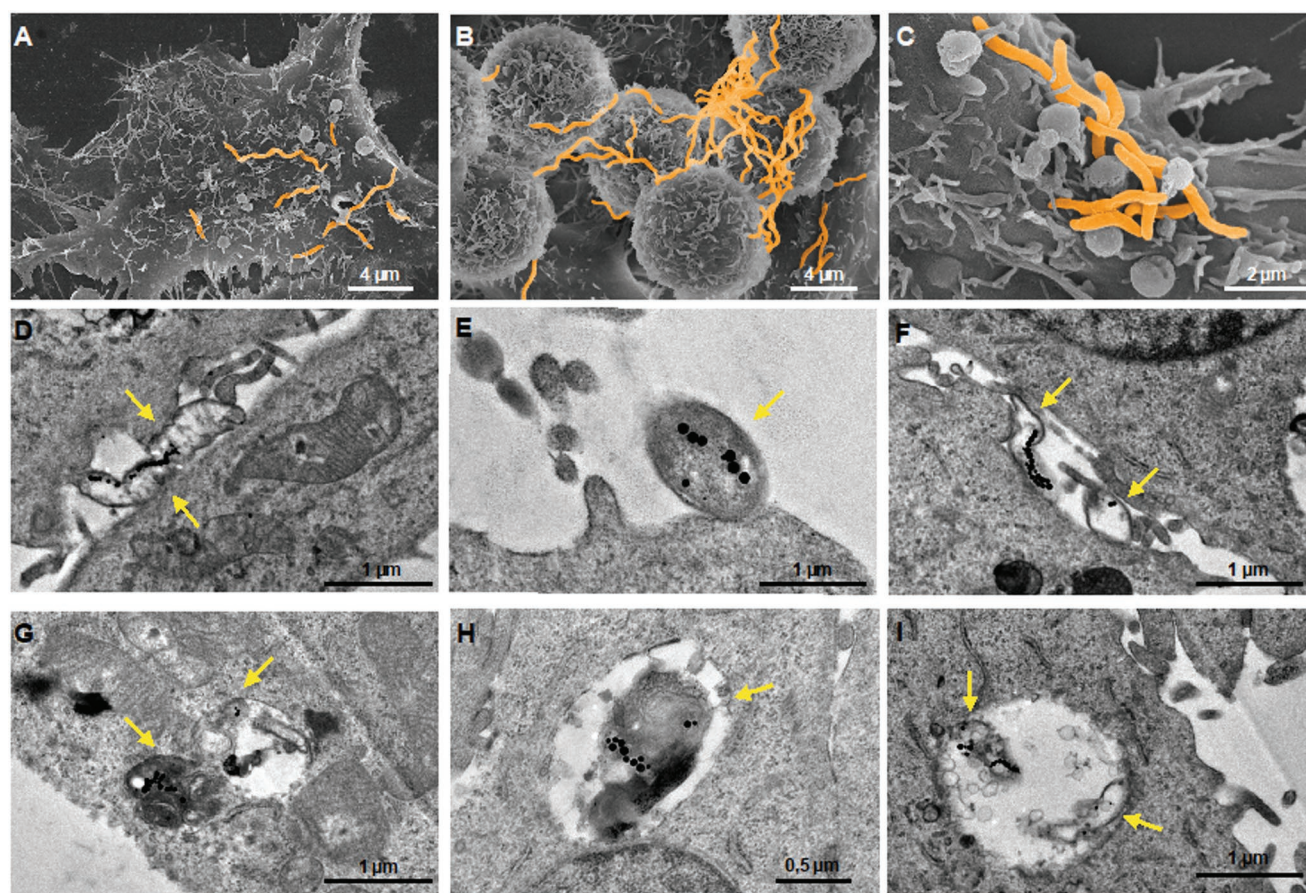
Despite the promising results exposed before, in order to use magnetotactic bacteria for cancer treatment we need to study how these agents interact with cancer cells: their cytotoxicity and the effect of the hyperthermia treatment on cancer cells. For this purpose, we have carried out an in vitro experiment in which we put in contact cells of *M. gryphiswaldense* MSR-1 with human lung A549 carcinoma cells (Figure 5). The cellular uptake of bacteria was visualized by fluorescence microscopy using labeled bacteria (Figure 6). This was possible due to the ability of the bacteria to show intrinsic red fluorescence when incubated with  $40 \times 10^{-6}$  M rhodamine 123 (red color, Figure 6b).<sup>[60]</sup> We also stained cells with Hoechst 33342 (blue color, Figure 6a) to visualize their nuclei. As shown in

Figure 6c, red bacteria are agglomerated in what could be the cancer cell cytoplasm, and surround the cell nuclei stained in blue.



**Figure 6.** Observation of human lung A549 carcinoma cells incubated for 4 h in the presence of *M. gryphiswaldense* MSR-1 using fluorescence microscopy. Bacteria were labeled with rhodamine and carcinoma cells were stained with Hoechst. a) Filter settings for Hoechst show nuclei in blue. b) Filter settings for rhodamine show bacteria in red. c) A merge image combining both filter settings. Scale bar = 10  $\mu$ m.





**Figure 7.** Electron micrographs of the interaction of *M. gryphiswaldense* with A549 carcinoma cells. A–C) SEM images showing bacteria adhered (in orange) on the cell surface. D–I) TEM images showing different steps of the internalization of bacteria. Yellow arrows indicate bacteria attached to cellular extensions D–F) and bacteria inside membrane bound vesicles in A549 cells G–I). The internalized bacteria are easily detectable in the cross-sections of the cells by the occurrence of associated magnetosomes.

blue after Hoechst staining. Therefore, we can infer that bacteria enter the cells but not their nuclei.

The interaction of *M. gryphiswaldense* bacteria with carcinoma cells was examined more closely by electron microscopy (Figure 7). After 24 h of contact, scanning electron microscopy (SEM) showed bacterial cells adhered on the cancer cell surface, both isolated and forming aggregates (Figure 7A–C). To have a better insight on how cells internalize these bacteria, we made ultrathin sections and visualized them under transmission electron microscopy (TEM). Figure 7 shows six steps of the bacterial invasion under TEM. There can be seen bacteria surrounded by cytoplasmic extensions (Figure 7D–F) and internalized bacteria located within endosome-like vesicles (Figure 7G–I). The bacteria could be identified because of the presence of magnetosomes.

The bacteria uptake process was further confirmed by magnetic measurements. The hysteresis loops of bacteria loaded carcinoma cells,  $M(H)$ , along with those of sole bacteria, allowed a quantitative estimation of the quantity of magnetite incorporated by carcinoma cells. This was possible by comparing the measured saturation magnetization,  $M_s$ , with that of bulk magnetite ( $M_s = 92.3 \text{ A m}^2 \text{ kg}^{-1}$ ). The actual mass of magnetite incorporated by the cells after 24 h of incubation

was of around 8–10 pg magnetite/cell, a very small percentage of what was initially added to the cell culture ( $\approx 50 \mu\text{g mL}^{-1}$ ). Unfortunately, with such low magnetite internalization we could not measure any SAR value with our hyperthermia systems in order to test if cell internalization had an impact on the heating efficiency of bacteria as it has been reported for isolated magnetosomes.<sup>[16]</sup>

To determine the potential cytotoxic effect that the bacteria could cause in cancer cells, we checked cell viability after 24 h and 48 h of the bacteria uptake. This was done using flow cytometry and Hoechst/propidium iodide staining to discriminate between living and dead cells. Hoechst is a blue membrane-permeable dye that links to DNA and therefore stains all the cell nuclei so that we can differentiate cells from other possible artefacts. Propidium iodide is a red stain that also links to DNA but only when the cell membrane is damaged indicating that those cells are no longer alive. The results of a representative experiment after 24 h of incubation are shown in Figure 8 where dead cells (the ones that incorporate propidium iodide) are defined inside the frame to be differentiated from the living ones. The percentage of dead cells in both control and cells incubated for 24 h with bacteria is similar suggesting that bacteria do not cause a cytotoxic effect on this carcinoma cell line.



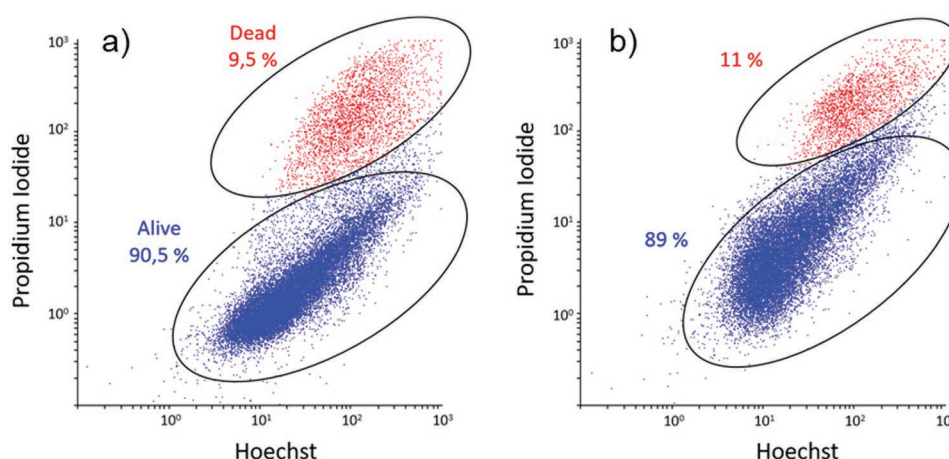


**Figure 8.** Fluorescence dot plots of Hoechst/propidium iodide stained cells obtained by flow cytometry in a representative experiment. a) Control cells. b) Cells after 24 h of bacteria uptake.

Combining the results from three different experiments we estimated the viability of the cell cultures, calculated as the ratio between the number of living cells and the total number of cells. We observed that viability is not affected with the uptake of *Magnetospirillum* bacteria as it always remained above 95%, 48 h after the bacteria uptake. Moreover, as observed in **Figure 9**, the presence of bacteria within cells does not affect their ability to grow. The evolution of the number of living cells over time shows the same pattern in both cell cultures with and without internalized bacteria, and no significant differences were found in the number of living cells after 48 h of the bacteria uptake. Different results were reported in previous experiments<sup>[35]</sup> for the isolated magnetosomes from *Magnetospirillum*, which can show cytotoxicity affecting both viability and cell proliferation.

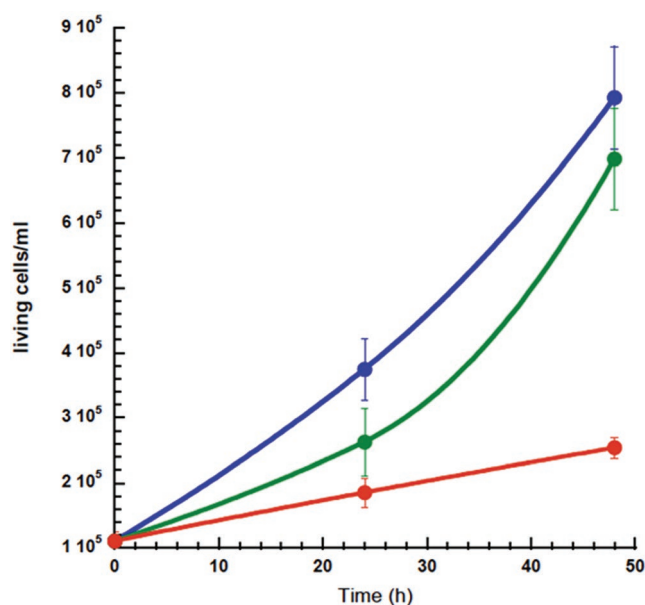


**Figure 9.** Time evolution of the number of live cells present in the culture after the bacteria uptake (in green) and hyperthermia treatment (in red). A control culture of cells without bacteria is also shown (in blue).

In the hyperthermia treatment, the bacteria loaded carcinoma cells were subjected to an AMF of 400 Oe and a frequency of 150 kHz during 45 min. A deleterious effect was observed immediately after AMF application. The results of a representative experiment are shown in **Figure 10**, which displays the propidium iodide fluorescence histograms of cells before and after AMF application. Before AMF application (Figure 10a,b) more than 98% of the cells showed low propidium iodine fluorescence level, corresponding to the cells that exclude propidium iodine or living cells. However, after AMF application (Figure 10c,d) the fluorescence histograms showed a bimodal distribution with a second peak in the region of high propidium iodine fluorescence level or dead cells. Considering the results of three independent experiments, the ratio of dead cells after the AMF exposure was estimated  $\approx 20\%$  of the total cells. Moreover, the cell proliferation was also strongly affected (see Figure 9). The growth of the cultures undergoing hyperthermia slowed down and at the end of the experiment, the number of living cells was three times lower than the control.

Therefore, our bacteria seem to be an interesting alternative to magnetosomes for hyperthermia treatments, since similar in vitro magnetic hyperthermia tests carried out with magnetosomes on cancer cells showed that isolated magnetosomes, contrary to our bacteria, had no impact on cancer cell viability.<sup>[16]</sup>

### 3. Conclusions

In this work we have proven that magnetotactic bacteria of the species *M. gryphiswaldense* are very promising as magnetic hyperthermia agents for cancer treatment. Calorimetric measurements reveal that these bacteria can increase the temperature of the medium up to the therapeutic window (40–45 °C) in less than 3 min by applying an external field with amplitude  $\geq 300$  Oe and frequency 300 kHz. Precisely, the alignment of the bacteria with the field maximizes their heating efficiency. This has been clearly seen in the AC hyperthermia measurements: hysteresis losses are maximized (reaching a nearly

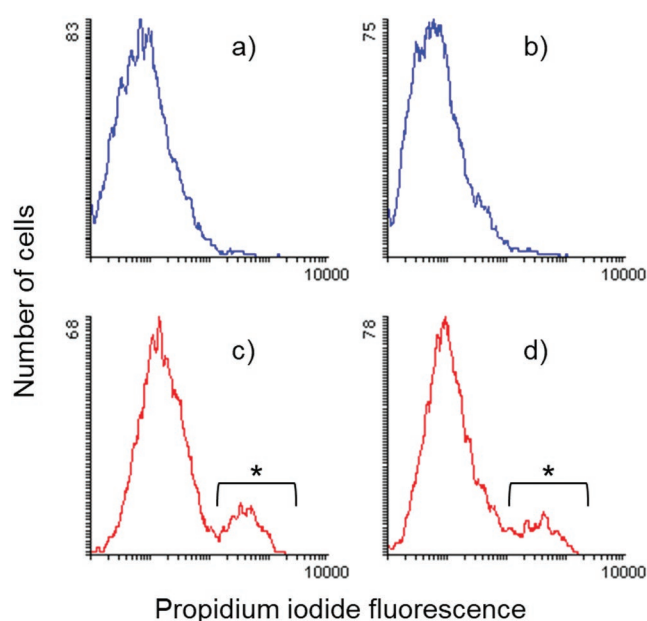


**Figure 10.** Fluorescence histograms of A549 cells stained with propidium iodide obtained by flow cytometer. a) Bacteria-loaded cells at the beginning of the experiment and b) 24 h later. c) Bacteria-loaded cells 2 h after AMF exposure (400 Oe, 150 kHz, and 45 min) and d) 24 h later. \* Region of dead cells in the frame.

optimum squared shape for the hysteresis loops) when the bacteria are parallel to the magnetic field. Moreover, the SAR values increase linearly with the magnetic field frequency,  $f$ , reaching a maximum SAR/ $f$  value of  $\approx 8 \text{ W g}^{-1} \text{ kHz}^{-1}$  at 350 Oe, which is appreciably greater than those obtained for isolated magnetosomes. Finally, the internalization and cytotoxicity of the bacteria in human lung carcinoma cells A549 has been assessed. Fluorescence microscopy images reveal that bacteria tend to agglomerate around the cancer cells, thereby exhibiting targeting capacity. In addition, SEM and TEM images clearly reveal that *M. gryphiswaldense* can be effectively uptaken by cancer cells, being incorporated into endosome-like vesicles.

Moreover, these bacteria do not affect the viability of the cell cultures, and they barely disturb the cell proliferation. However, both viability and cell proliferation seem to be strongly affected by the hyperthermia treatment. All these results indicate that magnetotactic bacteria are promising nanobots for cancer treatment.

## 4. Experimental Section

**Bacterial Strain and Growth Conditions:** *M. gryphiswaldense* MSR-1 (DMSZ 6631) was employed in this work. The strain was cultured in a standard medium as described elsewhere.<sup>[61]</sup> The medium was enriched with iron by adding  $100 \times 10^{-6} \text{ M}$  of Fe(III)-citrate. Cultures were carried out in three-fourths 1 L bottles at 28 °C without shaking for 120 h, when well-formed magnetosomes are observed. For all our studies the whole cells were employed. The bacteria were harvested by centrifugation, suspended in phosphate buffered saline (PBS), and fixed in 2% glutaraldehyde.

**Transmission Electron Microscopy:** Electron microscopy was performed on unstained cells adsorbed onto 300 mesh carbon-coated copper grids. TEM images were obtained with a JEOL JEM-1400 Plus

electron microscope at an accelerating voltage of 120 kV. The particle size distribution was analyzed using a standard software for digital electron microscope image processing, ImageJ.<sup>[62]</sup> For eukaryotic cell visualization, these were fixed overnight with 2% glutaraldehyde in 0.1 M Sörenson phosphate buffer. Then, they were washed several times with isoosmolar phosphate/sucrose buffer, dehydrated through an acetone series, and embedded in Epon Polarbed resin in beam capsules that polymerized at 55 °C in 48 h. A Leica UCT ultramicrotome was used to obtain ultrathin sections of 70 nm that were finally deposited onto carbon-coated copper grids.<sup>[63]</sup>

**Scanning Electron Microscopy:** Eukaryotic cells that were incubated for 24 h with *M. gryphiswaldense* were fixed with 2% glutaraldehyde in 0.1 M Sörenson phosphate buffer and dehydrated through increasing ethanol concentrations and hexamethyldisilazane. Finally, they were covered with gold under argon atmosphere, and visualized under the scanning electron microscope (Hitachi S-4800). To better differentiate between bacteria and cell microvilli, GIMP software was used to color the bacteria.

**Magnetic Hyperthermia:** Magnetic hyperthermia studies have been performed using a combination of calorimetric and AC magnetometry methods on two bacteria configurations: random and aligned. The calorimetric hyperthermia was carried out with a commercial 4.2 kW Ambrell Easyheat LI 3542 system working at fixed frequency, 300 kHz. Suspensions of bacteria with a total magnetite concentration of  $0.15 \text{ mg}_{\text{Fe}_3\text{O}_4} \text{ mL}^{-1}$  in distilled water and in 2% w/v agar were used for measurements and the AMF was tuned from 0 to 600 Oe. The agar was used to restrict the physical rotation of the bacteria by increasing the viscosity of the medium,<sup>[49]</sup> and also to align them in different orientations allowing us to study the effect of the alignment on their heating efficiency. AC magnetometry was carried out using a homemade setup.<sup>[64]</sup> The AMF amplitude was tuned between 0 and 400 Oe being the frequency 149, 300, and 528 kHz.

**Cytotoxicity Experiments and In Vitro Hyperthermia treatment:** These experiments were performed using A549 cell line from human lung carcinoma cells.<sup>[65]</sup> The cell line was propagated in RPMI medium supplemented with  $2 \times 10^{-3} \text{ M}$  L-glutamine, 10% fetal bovine serum, and a mixture of antibiotics ( $100 \text{ U mL}^{-1}$  penicillin and  $100 \mu\text{g mL}^{-1}$  streptomycin) and antimycotics ( $0.25 \mu\text{g mL}^{-1}$  amphotericin B) at 37 °C in a humidified atmosphere (95% relative humidity) and 5% CO<sub>2</sub>. For the cellular uptake of bacteria, cells were seeded at  $2 \times 10^5 \text{ cells mL}^{-1}$  in culture plates with RPMI medium containing  $5 \times 10^9 \text{ bacteria mL}^{-1}$  so that the ratio bacteria/cell will be around  $2.5 \times 10^4$ . After 24 h of incubation, cells were washed to remove the excess of bacteria not interiorized or attached to the cell surface, and they were incubated again with renewed RPMI for 24 h. Cell viability was measured at 24 and 48 h by flow cytometry on a Beckman Coulter Gallios cytometer using a mixture of Hoechst 33342 and propidium iodide (PI) so that dead cells Hoechst(+)/PI(+) could be distinguished from living cells Hoechst(+)/PI(−). A cell culture without bacteria was incubated concurrently as a control. To track the uptake of bacteria, a specific assay was repeated using fluorescent bacteria grown in a culture medium with  $40 \mu\text{g mL}^{-1}$  rhodamine 123. After the incubation with the fluorescent bacteria, the carcinoma cells were stained with Hoechst 33342 and observed under a Nikon Eclipse fluorescence microscope. For in vitro hyperthermia treatment, bacteria-loaded cells (after 24 h in contact) were exposed to an AMF of 400 Oe and a frequency of 150 kHz during 45 min, and cell viability was checked by flow cytometer, 2 and 24 h after the exposure. All experiments were performed three times and data are represented as the mean  $\pm$  standard deviation.

## Acknowledgements

D.G. and L.G. contributed equally to this work. The authors would like to thank Nanobioap cluster of excellence. Spanish Government is acknowledged for funding under the project number MAT2017-83631-C3. USF coauthors acknowledge support from U.S. Department of Energy, Office of Basic Energy Sciences under Award No. DE-FG02-07ER46438. The authors specially thank Prof. Ana García-Prieto for her critical revision of the article and her helpful suggestions.

## Conflict of Interest

The authors declare no conflict of interest.

## Keywords

cancer therapy, cytotoxicity, internalization, magnetic hyperthermia, magnetotactic bacteria

Received: May 21, 2019

Revised: July 24, 2019

Published online: August 27, 2019

- [1] K. Strebhardt, A. Ullrich, *Nat. Rev. Cancer* **2008**, *8*, 473.
- [2] R. P. Feynman, *Saturday Rev.* **1960**, *43*, 45.
- [3] Q. A. Pankhurst, J. Connolly, S. K. Jones, J. Dobson, *J. Phys. D: Appl. Phys.* **2003**, *36*, R167.
- [4] S.-N. Sun, C. Wei, Z.-Z. Zhu, Y.-L. Hou, S. S. Venkatraman, Z.-C. Xu, *Chin. Phys. B* **2014**, *23*, 037503.
- [5] V. Wagner, A. Dullaart, A. K. Bock, A. Zweck, *Nat. Biotechnol.* **2006**, *24*, 1211.
- [6] K. K. Jain, *Med. Princ. Pract.* **2008**, *17*, 89.
- [7] T. Neuberger, B. Schöpf, H. Hofmann, M. Hofmann, B. Von Rechenberg, *J. Magn. Magn. Mater.* **2005**, *293*, 483.
- [8] A. Ito, M. Shinkai, H. Honda, T. Kobayashi, *J. Biosci. Bioeng.* **2005**, *100*, 1.
- [9] C. Sun, J. S. H. Lee, M. Zhang, *Adv. Drug Delivery Rev.* **2008**, *60*, 1252.
- [10] G. Goya, V. Grazu, M. Ibarra, *Curr. Nanosci.* **2008**, *4*, 1.
- [11] G. A. O. Jinhao, G. U. Hongwei, X. U. Bing, *Acc. Chem. Res.* **2009**, *42*, 1097.
- [12] H. M. Williams, *Biosci. Horiz. Int. J. Stud. Res.* **2017**, *10*, hzx009.
- [13] D. Ortega Ponce, Q. Pankhurst, in *Nanoscience* (Ed: P. O'Brien), Royal Society of Chemistry, Cambridge **2012**, pp. 60–88.
- [14] E. A. Vitol, V. Novosad, E. A. Rozhkova, *IEEE Trans. Magn.* **2012**, *48*, 3269.
- [15] A. Espinosa, J. Kolosnjaj-Tabi, A. Abou-Hassan, A. Plan Sangnier, A. Curcio, A. K. A. Silva, R. Di Corato, S. Neveu, T. Pellegrino, L. M. Liz-Marzán, C. Wilhelm, *Adv. Funct. Mater.* **2018**, *28*, 1803660.
- [16] A. Plan Sangnier, S. Preveral, A. Curcio, A. K. A. Silva, C. T. Lefèvre, D. Pignol, Y. Lalatonne, C. Wilhelm, *J. Controlled Release* **2018**, *279*, 271.
- [17] S. J. Park, S. H. Park, S. Cho, D. M. Kim, Y. Lee, S. Y. Ko, Y. Hong, H. E. Choy, J. J. Min, J. O. Park, S. Park, *Sci. Rep.* **2013**, *3*, 3394.
- [18] G. M. Patel, G. C. Patel, R. B. Patel, J. K. Patel, M. Patel, *J. Drug Targeting* **2006**, *14*, 63.
- [19] N. S. Forbes, *Nat. Rev. Cancer* **2010**, *10*, 785.
- [20] D. A. Bazylinski, C. T. Lefèvre, B. H. Lower, in *Nanomicrobiology Physiological and Environmental Characteristics* (Eds: L. L. Barton, D. A. Bazylinski, H. Xu) Springer, New York **2014**, pp. 39–74.
- [21] R. P. Blakemore, *Annu. Rev. Microbiol.* **1982**, *36*, 217.
- [22] M. R. Benoit, D. Mayer, Y. Barak, I. Y. Chen, W. Hu, Z. Cheng, S. X. Wang, D. M. Spielman, S. S. Gambhir, A. Matin, *Clin. Cancer Res.* **2009**, *15*, 5170.
- [23] A. S. Mathuriya, *Crit. Rev. Biotechnol.* **2016**, *36*, 788.
- [24] O. Felfoul, M. Mohammadi, S. Taherkhani, D. de Lanaue, Y. Zhong Xu, D. Loghin, S. Essa, S. Jancik, D. Houle, M. Lafleur, L. Gaboury, M. Tabrizian, N. Kaou, M. Atkin, T. Vuong, G. Batist, N. Beauchemin, D. Radzioch, S. Martel, *Nat. Nanotechnol.* **2016**, *11*, 941.
- [25] S. Martel, M. Mohammadi, O. Felfoul, Zhao Lu, P. Pouponneau, *Int. J. Robotics Research* **2009**, *28*, 571.
- [26] E. Alphandéry, S. Faure, L. Raison, E. Duguet, P. A. Howse, D. A. Bazylinski, *J. Phys. Chem. C* **2011**, *115*, 18.
- [27] S. Martel, *Ther. Delivery* **2017**, *8*, 301.
- [28] S. Martel, *Biomicrofluidics* **2016**, *10*, 021301.
- [29] I. S. M. Khalil, M. P. Pichel, B. A. Reefman, O. S. Sukas, L. Abelmann, S. Misra, in *Proc. IEEE Int. Conf. on Robotics and Automation (ICRA)*, IEEE, Piscataway, NJ **2013**, pp. 5488–5493.
- [30] N. Mokrani, O. Felfoul, F. Afkhami Zarreh, M. Mohammadi, R. Aloyz, G. Batist, S. Martel, *Conf. Proc. IEEE Eng. Med. Biol. Soc.* **2010**, *2010*, 4371.
- [31] D. De Lanaue, O. Felfoul, J. P. Turcot, M. Mohammadi, S. Martel, *Int. J. Rob. Res.* **2014**, *33*, 359.
- [32] S. Rismani Yazdi, R. Nosrati, C. A. Stevens, D. Vogel, P. L. Davies, C. Escobedo, *Small* **2018**, *14*, 1702982.
- [33] E. A. Périgo, G. Hemery, O. Sandre, D. Ortega, E. Garaio, F. Plazaola, F. J. Teran, *Appl. Phys. Rev.* **2015**, *2*, 041302.
- [34] C. Blanco-Andujar, F. J. Teran, D. Ortega, in *Iron Oxide Nanoparticles for Biomedical Applications* (Eds: M. Mahmoudi, S. Laurent), Elsevier, Amsterdam **2018**, p. 197.
- [35] A. Muela, D. Muñoz, R. Martín-Rodríguez, I. Orue, E. Garaio, A. Abad Díaz de Cerio, J. Alonso, J. Á. García, M. L. Fdez-Gubieda, *J. Phys. Chem. C* **2016**, *120*, 24437.
- [36] E. Alphandéry, I. Chebbi, F. Guyot, M. Durand-Dubief, *Int. J. Hyperthermia* **2013**, *29*, 801.
- [37] C. Chen, L. Chen, Y. Yi, C. Chen, L.-F. Wu, T. Song, *Appl. Environ. Microbiol.* **2016**, *82*, 2219.
- [38] Z. Nemat, J. Alonso, I. Rodrigo, R. Das, E. Garaio, J. Á. García, I. Orue, M.-H. Phan, H. Srikanth, *J. Phys. Chem. C* **2018**, *122*, 2367.
- [39] S. Martel, M. Mohammadi, *Micromachines* **2016**, *7*, 97.
- [40] H. A. Hassan, M. Pichely, T. Hagemany, L. Abelmannyz, I. S. M. Khali, in *IEEE Int. Conf. on Intelligent Robots and Systems*, IEEE, Piscataway, NJ **2016**, pp. 5119–5124.
- [41] L. Marcano, A. García-Prieto, D. Muñoz, L. Fernández Barquín, I. Orue, J. Alonso, A. Muela, M. L. Fdez-Gubieda, *Biochim. Biophys. Acta, Gen. Subj.* **2017**, *1861*, 1507.
- [42] T. Ohguri, H. Imada, H. Narisada, K. Yahara, T. Morioka, K. Nakano, Y. Miyaguni, Y. Korogi, *Int. J. Hyperthermia* **2009**, *25*, 160.
- [43] J. van der Zee, D. González González, G. C. van Rhooen, J. D. van Dijk, W. L. van Putten, A. A. Hart, *Lancet* **2000**, *355*, 1119.
- [44] Y. Zhang, W. Zhang, C. Geng, T. Lin, X. Wang, L. Zhao, J. Tang, *Prog. Nat. Sci.* **2009**, *19*, 1699.
- [45] R. Hergt, S. Dutz, *J. Magn. Magn. Mater.* **2007**, *311*, 187.
- [46] I. Andreu, E. Natividad, *Int. J. Hyperthermia* **2013**, *29*, 739.
- [47] C. Martinez-Boubeta, K. Simeonidis, A. Makridis, M. Angelakeris, O. Iglesias, P. Guardia, A. Cabot, L. Yedra, S. Estradé, F. Peiró, Z. Saghi, P. a Midgley, I. Conde-Leborán, D. Serantes, D. Baldomir, *Sci. Rep.* **2013**, *3*, 1652.
- [48] K. Simeonidis, M. P. Morales, M. Marciello, M. Angelakeris, P. de la Presa, A. Lazaro-Carrillo, A. Tabero, A. Villanueva, O. Chubykalo-Fesenko, D. Serantes, *Sci. Rep.* **2016**, *6*, 38382.
- [49] D. Serantes, K. Simeonidis, M. Angelakeris, O. Chubykalo-Fesenko, M. Marciello, M. Del Puerto Morales, D. Baldomir, C. Martinez-Boubeta, *J. Phys. Chem. C* **2014**, *118*, 5927.
- [50] R. Das, J. Alonso, Z. Nemat, P. Porshokouh, V. Kalappattil, D. Torres, M.-H. Phan, E. Garaio, J. Á. García, J. L. Sanchez Llamazares, H. Srikanth, *J. Phys. Chem. C* **2016**, *120*, 10086.
- [51] I. Conde-leboran, D. Baldomir, C. Martinez-boubeta, O. Chubykalo-fesenko, M. Del, P. Morales, G. Salas, D. Cabrera, J. Camarero, F. J. Teran, D. Serantes, *J. Phys. Chem. C* **2015**, *119*, 15698.
- [52] A. C. V. Araujo, F. Abreu, K. T. Silva, D. A. Bazylinski, U. Lins, *Mar. Drugs* **2015**, *13*, 389.



- [53] A. Lohße, I. Kolinko, O. Raschdorf, R. Uebe, S. Borg, A. Brachmann, J. M. Plitzko, R. Müller, Y. Zhang, D. Schüler, *Appl. Environ. Microbiol.* **2016**, *82*, 3032.
- [54] I. Orue, L. Marcano, P. Bender, A. García-Prieto, S. Valencia, M. A. Mawass, D. Gil-Cartón, D. Alba Venero, D. Honecker, A. García-Arribas, L. Fernández Barquín, A. Muela, M. L. Fdez-Gubieda, *Nanoscale* **2018**, *10*, 7407.
- [55] P. Guardia, R. Di Corato, L. Lartigue, C. Wilhelm, A. Espinosa, M. Garcia-Hernandez, F. Gazeau, L. Manna, T. Pellegrino, *ACS Nano* **2012**, *6*, 3080.
- [56] E. C. Abenojar, S. Wickramasinghe, J. Bas-Concepcion, A. C. S. Samia, *Prog. Nat. Sci.: Mater. Int.* **2016**, *26*, 440.
- [57] L. C. Branquinho, M. S. Carrião, A. S. Costa, N. Zufelato, M. H. Sousa, R. Miotto, R. Ivkov, A. F. Bakuzis, *Sci. Rep.* **2013**, *3*, 2887.
- [58] B. Gleich, J. Weizenecker, *Nature* **2005**, *435*, 1214.
- [59] A. Kraupner, D. Eberbeck, D. Heinke, R. Uebe, D. Schüler, A. Briel, *Nanoscale* **2017**, *9*, 5788.
- [60] E. Alphonché, D. Abi Haidar, O. Seksek, F. Guyot, I. Chebbi, *Nanoscale* **2018**, *10*, 10918.
- [61] M. L. Fdez-Gubieda, A. Muela, J. Alonso, A. García-Prieto, L. Olivi, R. Fernández-Pacheco, J. M. Barandiarán, *ACS Nano* **2013**, *7*, 3297.
- [62] C. A. Schneider, W. S. Rasband, K. W. Eliceiri, *Nat. Methods* **2012**, *9*, 671.
- [63] A. García-Prieto, J. Alonso, D. Muñoz, L. Marcano, A. Abad Díaz de Cerio, R. Fernández de Luis, I. Orue, O. Mathon, A. Muela, M. L. Fdez-Gubieda, *Nanoscale* **2016**, *8*, 1088.
- [64] E. Garaio, J. M. Collantes, F. Plazaola, J. A. Garcia, I. Castellanos-Rubio, *Meas. Sci. Technol.* **2014**, *25*, 115702.
- [65] D. J. Giard, S. A. Aaronson, G. J. Todaro, P. Arnstein, J. H. Kersey, H. Dosik, W. P. Parks, *JNCI, J. Natl. Cancer Inst.* **1973**, *51*, 1417.